Journal of Marine Research, 48, 223–253, 1990

Journal of
MARINE RESEARCH

Volume 48, Number 2

Effects of large-scale topography on abyssal circulation

by David N. Straub[1] and Peter B. Rhines[1]

ABSTRACT

Two models are employed to study the effect of topographically induced planetary islands (i.e. closed contours of potential vorticity) on the abyssal circulation of an ocean basin. The first is a steady state calculation using a 1½ layer model of the abyssal ocean forced by a uniform upwelling. Planetary geostrophic dynamics yield a characteristic equation in which the inverse potential vorticity serves as a streamfunction for the characteristic velocity field. Aside from warping the classic Stommel-Arons flow in the immediate vicinity of the planetary island, the topography introduces two new elements to the zonal flow west of the topography. The first of these is a system of two zonal jets, flowing in opposite directions and centered on the separatrix contour. The second is an acceleration (or retardation) of the zonal flow (with respect to the classic flat-bottom result) in a broader region of the basin. The strengths of both the double jets and the broader regions of enhanced/retarded zonal flow are found to be determined by forcing in relatively small areas of the basin. The former are excited in the vicinity of saddle points of potential vorticity whereas the latter are excited primarily where the curvature of potential vorticity contours is large.

The second model, a time dependent 2½ layer planetary geostrophic model is then used to investigate the spin-up problem. The model is forced by a uniform upwelling through each of the two interfaces. The density jump at the upper interface (e.g. the thermocline) is chosen to be ten times that at the lower interface, a disparity which leads to a separation in time scale between the fast and the slow waves of the system. Topography, however, induces a strong coupling between these two modes and results in a quick baroclinization of the flow over the topography. This baroclinization occurs well before the arrival of the nondispersive wave front from the eastern boundary and thus differs from the traditional view of spin-up.

1. School of Oceanography, University of Washington, WB-10, Seattle, Washington, 98195, U.S.A.

1. Introduction

In their classic 1960 paper, Stommel and Arons (SA) modeled the steady abyssal circulation using a single layer planetary-geostrophic model with a uniform vertical velocity through the upper interface. Given the rigid lid approximation, lack of topography and linearized dynamics, the potential vorticity contours in their model were strictly zonal. The specified vertical fluxes through the interface determined the meridional velocities locally through the Sverdrup relation. Zonal velocities, by contrast, represent the unforced (or free) part of the flow and hence are not determined locally. They are found only upon integration of a characteristic equation from the eastern boundary and are determined by meridional gradients in the characteristic speed as well as in the basin's breadth.

Sea floor basins and ridges introduce planetary islands (i.e. closed contours) of potential vorticity (Q), Welander (1969). Outside of the planetary islands, specified vertical fluxes through the interface determine the component of velocity perpendicular to the now convoluted potential vorticity contours through the topographic Sverdrup relation. Similarly, the free flow is no longer strictly zonal but rather is tangent to potential vorticity contours.

In Section 2, a steady state problem similar to that discussed by Welander is examined. Planetary geostrophic dynamics lead to a characteristic equation in which the characteristic velocity is closely related to the potential vorticity field. This equation is then numerically integrated in two 2500 km square beta-plane basins, each containing a planetary island of Q (in one case due to a Gaussian bump of topography and in another due to a Gaussian depression of the sea floor). Forcing by a prescribed (uniform) vertical velocity leads to significant modifications of the classic flat bottom circulation, not only in the immediate vicinity of the topography, but also to its west. The origins of these new elements of the flow are discussed.

The spin up of the SA circulation has been addressed by Kawase (1987) with a $1\frac{1}{2}$ layer primitive equation model forced by a local mass source in the northwest corner of the basin. The source excites Kelvin waves (Davey, 1983; Kawase, 1987) which serve to raise the interface height field on the perimeter of the basin and at the equator. The poleward and eastward interior drift is established upon the arrival of baroclinic planetary Rossby waves, carrying information of these boundary events to the interior of the basin.

Section 3 treats the time dependent problem, essentially adding the effects of topography and stratification to Kawase's (1987) spin-up solution. The model is interpreted as representing the fast (0(10 yrs.)) spin-up to a quasi-steady state in which the abyssal layer is slowly filling. Treatment is restricted to the planetary-geostrophic component of the problem, using a $2\frac{1}{2}$ layer time dependent planetary-geostrophic model similar to the $1\frac{1}{2}$ layer model of Rhines (1989). The density jump between the inactive upper ocean and the upper active layer was chosen to be ten times that between

the two active layers. Thus, the model may be interpreted as having a middle layer separated from an abyssal layer by a weak density jump and from an inactive upper ocean by a stronger density jump (e.g., a thermocline).

2. The steady state problem

a. Model description. The steady state model has one dynamically active abyssal layer below an infinite (inactive) upper ocean. The abyssal layer is thick enough to completely cover the topography. In accord with planetary-geostrophic dynamics, it is assumed that (1) the horizontal velocities are geostrophic, (2) the three dimensional velocity field is nondivergent, (3) the pressure is hydrostatic and (4) relative vorticity is negligible. If, in addition, the upper layer is assumed to be at rest, the velocity field in the abyssal layer is given by

$$\mathbf{u} = (u, v) = \left(-\frac{g'}{f}\eta_y, \frac{g'}{f}\eta_x\right) \tag{1}$$

where η is the interface height field, g' is the reduced gravity and x and y are the standard Cartesian coordinates. The Coriolis frequency is taken to be $f = f_o + \beta y$, an approximation which applies best to low latitudes where the convergence of meridians is small. The approximation remains reasonably accurate even at high latitudes, however, with the absence of latitudinal dependence in β largely compensating for the absence of latitudinal dependence is distance between meridians.[2]

In general, the vertical velocity is given by

$$w_t = w_i + \mathbf{u} \cdot \nabla\eta \tag{2}$$

at the top of the abyssal layer and by

$$w_b = \mathbf{u} \cdot \nabla h, \tag{3}$$

where h is the topographic height field, at the bottom. The diapycnal component, w_i, of w_t is taken to be a known constant. Together with the incompressibility and hydrostatic assumptions, Eqs. (1–3) combine to yield

$$\mathbf{u} \cdot \nabla\Pi = \frac{-w_i}{f} \tag{4}$$

When the upper layer is assumed to be at rest, (4) can be rewritten as

$$g'J(\eta, \Pi) = -w_i \tag{5}$$

2. The characteristic speed away from topography is proportional to β (see below), which, in spherical geometry is proportional to cosine (latitude), as is the distance between meridians. The approximations of constant β and of constant distance between meridians thus nullify one another in that there is no net effect of the 'time of travel' between meridians, moving at the characteristic velocity.

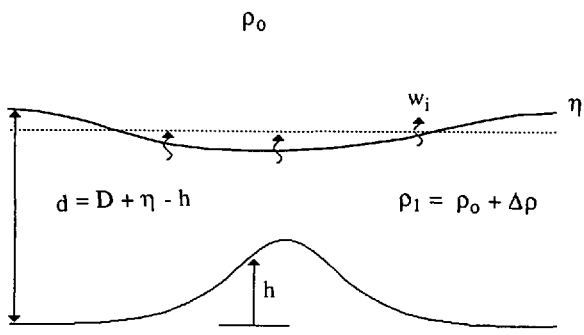

Figure 1. Sketch of model setup. The model is dynamically active in the abyssal layer only, thus effects of the diapycnal mass flux on the horizontal velocity field of the upper layer are ignored. The bottom topography, h, is assumed to be everywhere submerged in the abyssal layer. $w_i = 4 \times 10^{-7}$ m/s is the diapycnal component of the vertical velocity at the interface and $g' = .049$ m/s^2 is the reduced gravity.

where

$$\Pi = 1/Q = d/f \tag{6}$$

is the inverse potential vorticity, $J(,)$ is the Jacobian operator and $d = D + \eta - h$ is the total depth of the abyssal layer (see Fig. 1 for model set-up).

Eq. (5) can be rewritten as a characteristic equation for the interface height field, η

$$\mathbf{c} \cdot \nabla\eta = -w_i \tag{7}$$

in which the characteristic velocity, $\mathbf{c}$, is given by

$$\mathbf{c} = g'(\Pi_y, -\Pi_x). \tag{8}$$

Characteristic contours are then defined as the curves which would be traced out by an observer moving with the characteristic velocity and are coincident with potential vorticity contours. The inverse potential vorticity, Π, is proportional to a stream function for $\mathbf{c}$.[3]

The interface height field in the interior is found by integrating (7) from an "eastern" boundary, when η may be taken to be zero:

$$\eta = \int_0^\lambda \frac{-w_i}{c} d\lambda' = -\int_0^\lambda F d\lambda' \tag{9}$$

where $F = w_i/c$, $c = |\mathbf{c}|$ and λ is the distance, following a characteristic, from the

3. Since $J(\eta,\eta)$ is identically zero, $\mathbf{c}$ is not uniquely defined in that any vector of the form $A(-\eta'_y,\eta'_x)$ may be added without changing the validity of (7). Note also that in the absence of topography, (8) yields the familiar expression $\mathbf{c} = \hat{\imath}(-\beta g' d/f^2)$.

eastern boundary to a point in the interior. As in SA, the details of the boundary layers are left unresolved.

b. Model results. Figure 2a shows Π contours (which are both geostrophic contours and characteristics) for a basin containing an isolated planetary island of Q. The basin is a 2500 km square northern hemisphere beta-plane and topography is in the form of a symmetric Gaussian bump with a horizontal length scale of 380 km centered in the basin. The reduced gravity, g', is 0.049 m/s^2 and the mean depth is 1000 m. The separatrix contour, delineating the outer edge of the planetary island is sketched as a dashed curve. Values of Π generally decrease from south to north as well as from the perimeter to the interior of the planetary island and the point at which the separatrix contour crosses itself is a saddle point in Π. Because c is proportional to $|\nabla\Pi|$ the integrand of (9) is singular at the saddle point. This singularity is nonremovable, precluding integration of (9) from the saddle point westward along the separatrix contour. An appeal to higher order processes in the immediate vicinity of this point is therefore necessary to solve the problem completely. Nonetheless, it is interesting to examine the purely inviscid, planetary geostrophic solution where it exists (outside of the closed contours and off of the western segment of the separatrix contour).

Figure 2b shows contours of F, the integrand of (9). Extreme values near the singularity as well as values inside the planetary island have been omitted. A striking feature of the plot is the breadth of the region of high F near the critical point. Though planetary geostrophic dynamics fail in the immediate vicinity of the singularity, there exists a broader neighborhood about the critical point in which values of F are large with respect to those in the remainder of the basin and in which planetary geostrophic dynamics may well hold. Characteristics which pass through this region (i.e. characteristics close to the separatrix contour) exit with much lower (more negative) values of η than their neighbors which pass to the side of or just graze the region. Thus, west of the saddle point, characteristics nearer the separatrix contour exhibit lower values of η than those slightly farther away. A minimum in the η field is thus expected to lie along the seperatrix contour.

Figure 2c shows the η field found by integrating (9) numerically. Values inside the closed contour region are omitted because they are not determined by the present theory. As anticipated, there is a minimum in η extending from the saddle point westward along the separatrix contour. The associated thermal wind shear is a system of two jets, flowing in opposite directions and connecting the western boundary layer (WBL) to the planetary island. The eastward jet leaves the WBL and flows toward the saddle point where it turns southward and continues around the closed contours. After circumnavigating the planetary island, it then returns to the WBL as the northern branch of the double jet system. Individual streamlines, however, may leave the westward jet to feed the more traditional poleward and eastward drift to the north.

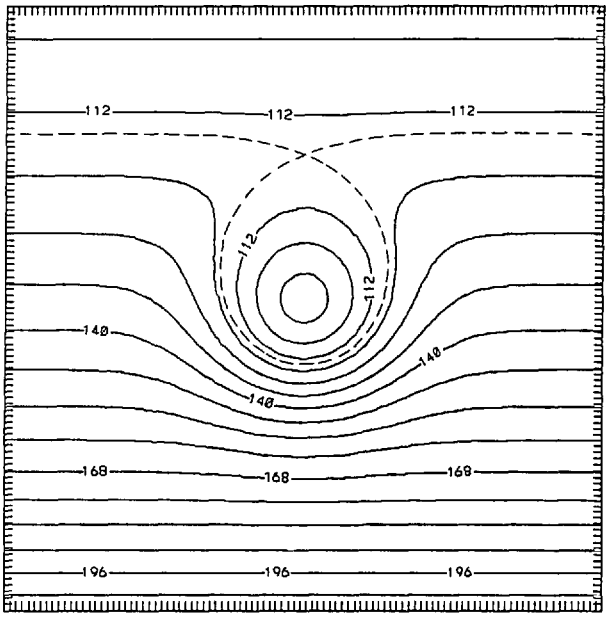

Figure 2. (a) Contours of $\Pi_{rest} = (D - h)/(f_o + \beta y)$ in a 2500 km by 2500 km basin. The topography, h, is a Gaussian bump, $h = h_o \exp(-a^2(x^2 + y^2))$ where h_o is 300 m and $1/a$ is 380 km. Other parameters are as follows: $f_o = .73 \times 10^{-4} s^{-1}$, $\beta = 2 \times 10^{-11} m^{-1} s^{-1}$ and $D =$ 1000 m. The separatrix contour has been sketched in as a dashed line. (b) Contours of $F = w_i/c$. Extreme values (near the singularity) have been omitted as have values inside the closed contour region. (c) The corresponding interface height field, η, measured in meters (again, the values inside the closed contour region have been omitted). Note the double jet structure centered on the separatrix contour and the relatively quick zonal flow west of the topography.

To the north, south and east of any significant topography, the flow is nearly identical to that predicted by SA theory for a flat-bottom basin (for comparison, the flat bottom result is shown in Fig. 3). To the west of the topography, and south of the double jet structure, the free component of flow continues to differ from the corresponding flat-bottom result (it is accelerated in the north and retarded in the south). This effect is not related to the saddle point, but rather to the variation in integration path length with increasing Q. With increasing Q the lengthening paths reinforce the increase in F due to the decreasing characteristic speed. The net result is an enhancement (with respect to the flat-bottom result) of the meridional pressure gradient and zonal velocity in this region.

Figures 4a–c are analogous to Figures 2a–c for a second example in which the closed contours are formed by a topographic low (which might be taken as a crude representation of a deep basin). Once again, there is a system of two jets located between the WBL and the saddle point (south of the closed contours in this case) and connected by a jet around the perimeter of the closed contours. Notice, however, that the horizontal

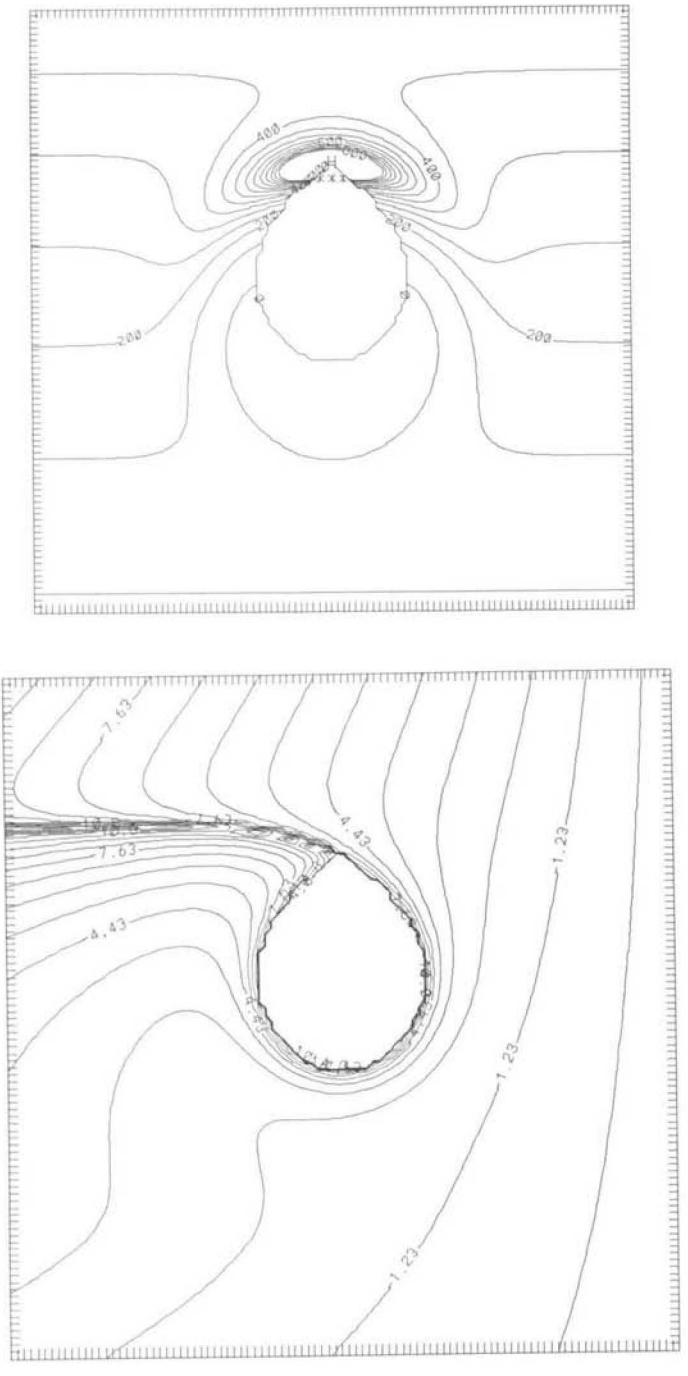

Figure 2. (Continued)

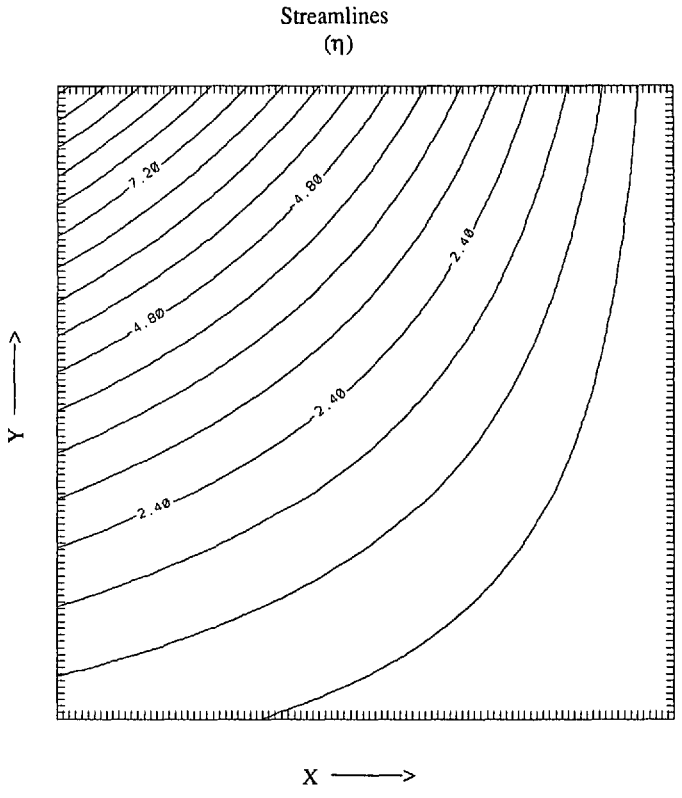

Figure 3. Same as 2c, but for the flat bottom case.

extent of the region of large F near the critical point is smaller than that in the previous example. Presumably, therefore, the double jet here is more likely to be weakened or eradicated by higher order effects than before. Note also that the zonal flow west of the closed contours, instead of being enhanced as before, is diminished to the point of being westward in the south before increasing to an eastward flow equal in magnitude to that of the flat bottom case near the northern limit of the topography. In contrast with the previous example path lengths here decrease with increasing Q, while F increases with Q as before. The net result is the weak meridional gradient of the interface height field (and weak zonal flow) seen west of the topography.

Figure 5 compares pressure along a meridian near the western boundary for the three cases. Both the systems of double jets (seen as spikes in the pressure curves) and the broader enhancement/retardation of zonal flow represent nonlocal effects of the topography on the flow west of the topography. Such influences are largely restricted to the free component of flow.[4] While it is clear that the double jets are excited by forcing

4. The forcing locally determines $\mathbf{u} \cdot \nabla \Pi$ through (4). To the extent that steepening effects remain small, $\nabla \Pi$, as well as the right hand side of (4), is known a priori and the "forced" component of flow is determined.

near the saddle point, it is not yet clear where forcing in the interior leads to the broader regions of enhanced/retarded zonal flow observed west of the topography.

c. Excitation of the free component of flow. We would like to determine, more locally, where forcing leads to an excitation of the free component of flow. Otherwise stated, where would slight changes in the forcing field, w_i, result in disproportionately large changes in the flow parallel to Q contours? Let μ denote the component of this component of the velocity vector;

$$\mu = \frac{-\mathbf{u} \cdot (\hat{\mathbf{k}} \times \nabla Q)}{|\nabla Q|} \tag{10}$$

where $\hat{\mathbf{k}}$ is the vertical unit vector. As before, λ will be used to denote distance, following a characteristic, from the eastern boundary. If the orthogonal coordinate is denoted by n, μ is given by

$$\mu = \frac{g'}{f} \eta_n. \tag{11}$$

Thus, for forcing to have an effect on the free flow, it must result in changes in η_n.

To see how and where η_n results from forcing in the interior, we consider changes in η_n along a characteristic. Using (9),

$$\frac{\partial}{\partial \lambda} \eta_n = \frac{\partial}{\partial \lambda}\left[\frac{\partial}{\partial n} \int_\lambda^0 F d\lambda'\right] \tag{12}$$

which, after some algebra leads to

$$\eta_n = \int_0^\lambda (F_n + \kappa F)\, d\lambda' \tag{13}$$

where κ is the curvature[5] of the Π contours, a locally measured quantity. Thus, following a characteristic, the pressure gradient responsible for the free flow is altered both by spatial variations in F and by curvature in the potential vorticity field.

Plots of the integrand of (13), corresponding to Figures 2 and 4, are shown in Figures 6a,b. Following a characteristic, these fields describe changes in the pressure gradients responsible for the free flow. Values inside the closed contour region and extreme values near the critical point have been omitted. It is interesting to note that the free flow may depend primarily on forcing in rather limited regions. This suggests that the long-geostrophic contour component of the flow, as calculated using averaged upwelling values based on global budgets, may differ drastically if local variability in the forcing were taken into account. Specifically, variability in the forcing in regions of

5. Curvature is defined as the derivative of ϕ with respect to arclength, where ϕ is the angle between the tangent to the curve and some line of reference.

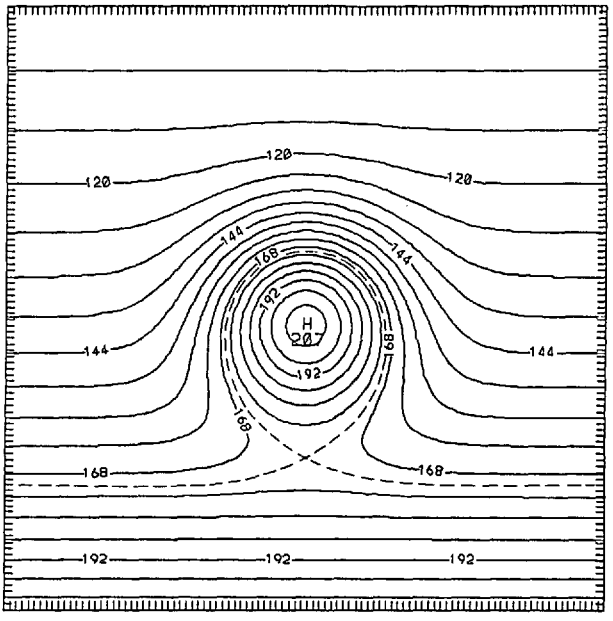

Figure 4. Same as 2 except that $h_o = -500$ m. Here the singularity (and hence the double jet) occurs to the south of the planetary island. In contrast to the first example, the zonal flow to the west of the topography is weakened with respect to the flat bottom case. In fact, a weak westward drift is observed. Note also that the region of large F surrounding the saddle point is much reduced in this case.

curved Q contours would have a particularly large effect on the free flow both locally and to the "west" of those regions. By contrast, such variability only locally affects the cross-contour component of flow.

3. The spin-up problem

In Kawase's spin-up calculation (Kawase, 1987), the interior flow was established by the arrival of a nondispersive baroclinic Rossby wave from the eastern boundary. In the steady state, a distributed sink provided by a Newtonian damping of the interface height field forced the interior poleward flow. In the limit of very weak or no damping, however, this interior drift can be established long before the steady state is reached. Thus, there exists a quasi-steady state in which the interior flow is like that of the SA solution and in which the basin is gradually filling. Similarly, if the source is turned off or weakened, there would be a quasi-steady state in which the basin is draining. In this case, the interior drift would be equatorward and westward. It is the spin up (of order 10 yrs.) to such a quasi-steady state that is addressed here.

The addition of topographically induced planetary islands to Kawase's 1½ layer model leads to a distortion of the wave front as it traverses the topography and, of

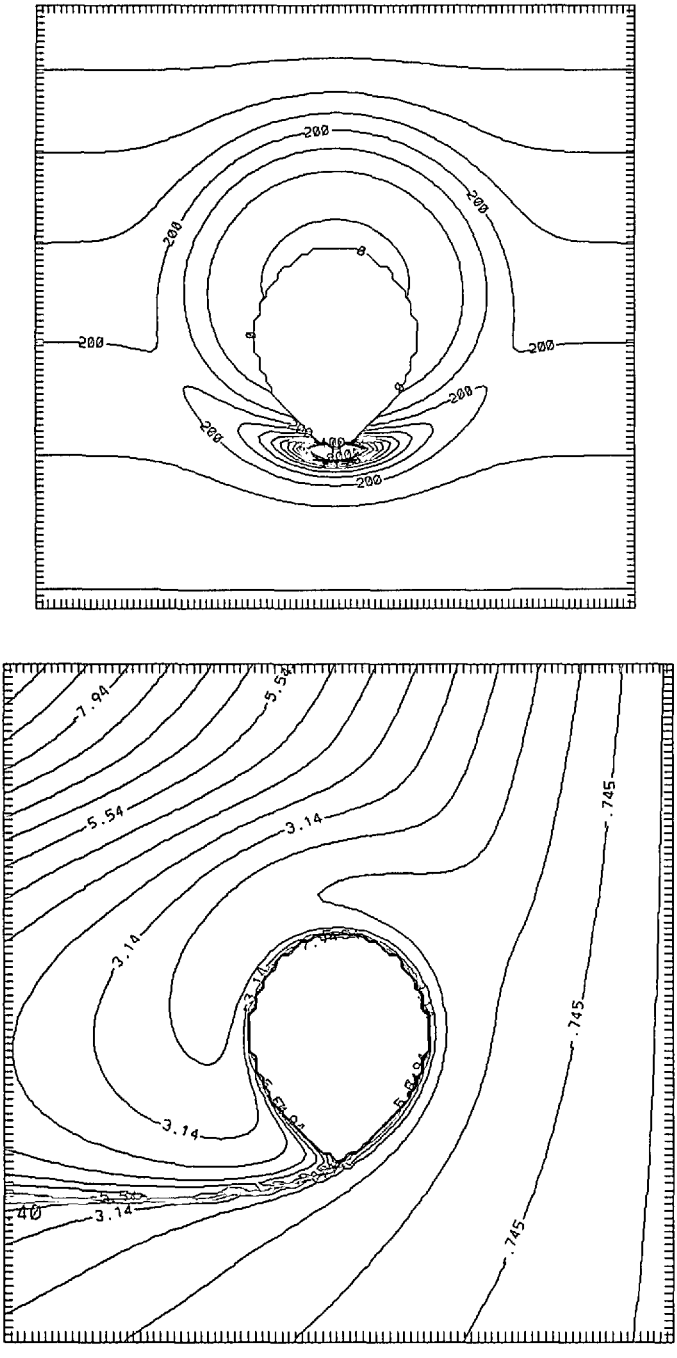

Figure 4. (Continued)

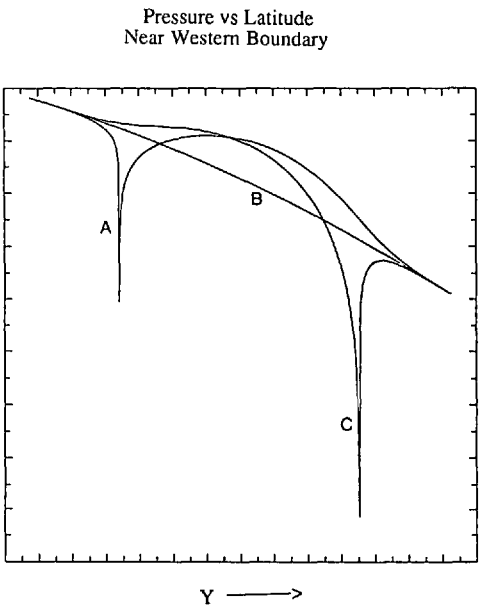

Figure 5. Pressure contours along a meridian near the western boundary for the three cases. The curve marked with an "a" corresponds to Figure 4, the monotonic curve (marked with a "b") corresponds to Figure 3 and the curve marked with a "c" corresponds to Figure 2.

course, to a different set of dynamics inside the closed contour region. The combined effect of topography and stratification alters the problem still further, introducing baroclinity to the interior well before the arrival of the baroclinic front from the eastern boundary.

a. Model description. A 2½ layer planetary geostrophic model is used to isolate the planetary wave component of the problem, while adding some of the effects of stratification and topography. The model forcing is chosen to be a uniform upwelling, equal in strength through each of the two interfaces. Since the Kelvin wave speed is large compared to the Rossby wave speed, the net effect of the former is modeled as a uniform uplifting of interface height field along the boundary. Over the time scales considered here, this is nearly equivalent to holding the interface height fixed on the boundary while imposing a uniform sink on the interior. In this sense, the model forcing corresponds to forcing by a mass source in the abyssal layer (i.e. a transfer of mass from the inactive layer to the abyssal layer).

The model is similar to a 1½ layer model used by Rhines (1989) to examine baroclinic adjustment of free flow in a repeating channel configuration. Here, an additional layer is appended and the model is used in a basin configuration similar to that in the first steady state example, (see Fig. 7 for model details). The initial flow field is zero everywhere. Time dependence is introduced through the stretching term in the

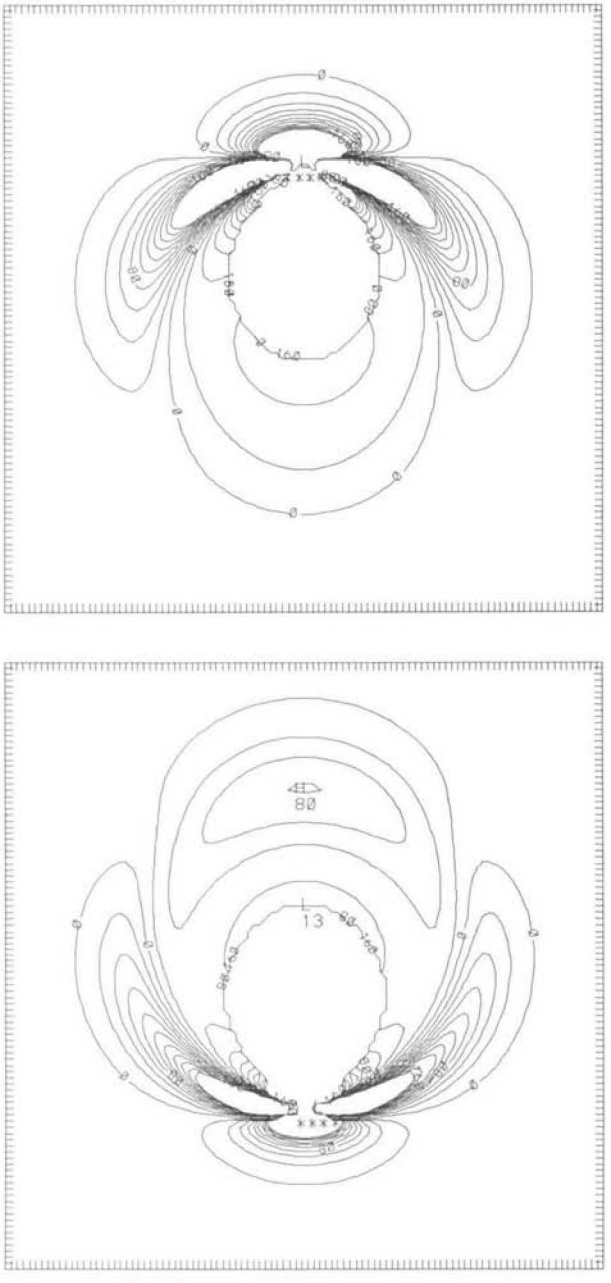

Figure 6. Contours of the integrand of (13): (a) corresponding to Figure 2 and (b) corresponding to Figure 4. Following a characteristic, this field describes how the pressure gradient perpendicular to the characteristic (and hence proportional to the free flow) changes. Note that most of the change following a particular characteristic may occur in a relatively restricted area.

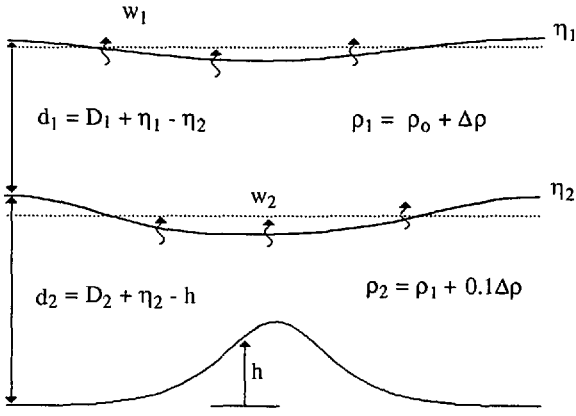

Figure 7. Sketch of the time dependent model set up. The inactive upper ocean, assumed to be at rest, is separated from the upper active layer by a density jump ten times that separating the two active layers. This difference leads to a large disparity between the fast and slow waves of the system and tends to force the system toward compliance with the topographic Sverdrup relation on the faster of the two time scales. Topography, h, is given by $h = h_o \exp(-a^2(x^2 + y^2))$ where $1/a$ is about 380 km, $h_o = 300$ m and the basin is a 2500 km. square beta plane. The reduced gravities are $g_1 = 0.05$ m/s^2 and $g_2 = 0.005$ m/s^2, respectively. D_1 and D_2 are both 1000 m, $\beta = 2 \times 10^{-11}$m^{-1}s^{-1} and $f_o = .73 \times 10^{-4}$s^{-1}. The numerical calculation solves 14a,b on a 100 × 100 grid.

potential vorticity equations, written here in a form analogous to Eq. (5):

$$\eta_{1t} - \eta_{2t} + g_1 J(\eta_1, \Pi_1) = w_2 - w_1 - R\nabla^2\eta_2 \tag{14a}$$

and

$$\eta_{2t} + g_1 J(\eta_1 + \epsilon\eta_2, \Pi_2) = -w_2 + 2R\nabla^2\eta_2 + \frac{R}{\epsilon}\nabla^2\eta_1 \tag{14b}$$

where the subscripts 1 and 2 refer to the upper and lower active layers respectively and $\epsilon = g_2/g_1$ is the ratio of the two reduced gravities. Other notation is as before except that a weak Laplacian diffusion ($R = 40$ m^2/s) of the interface height fields, corresponding roughly to the combined effects of both an internal and a bottom Ekman layer has been added.

The density jump between the inactive layer and the upper active layer is chosen to be ten times that between the two active layers (i.e. $g_1 = 10g_2$). This disparity provides for a separation of timescales in the adjustment process. The fast adjustment, essentially an adjustment of the upper interface, is described by the sum of 14a,b:

$$\eta_{1t} + g_1 J(\eta_1, \Pi_b) = -g_2 J(\eta_2, \Pi_2) - w_1 + R\nabla^2\eta_2 + \frac{R}{\epsilon}\nabla^2\eta_1 \tag{15}$$

where $\Pi_b = \Pi_1 + \Pi_2 = (d_1 + d_2)/f$. From the second term on the LHS, we see that

the relevant wave speed for the fast mode is of order $g_1|\nabla\Pi_b|$, or

$$c_1 \approx \frac{\beta g_1 d_T}{f^2} \approx .4 \text{ m/s}. \tag{16}$$

where $d_T = d_1 + d_2$. Similarly, the wave speed associated with the slower adjustment is given by

$$c_2 \approx \frac{\beta g_2 d_1 d_2}{d_T f^2} \approx .01 \text{ m/s}. \tag{17}$$

There are thus three basic timescales in the problem; one associated with each of the wave speeds and a third associated with the diffusion. These are

$$T_1 \approx \frac{L}{c_1} \approx 1 \text{ month}, \tag{18a}$$

$$T_2 \approx \frac{L}{c_2} \approx 3 \text{ years} \tag{18b}$$

and

$$T_3 \approx \frac{L^2}{R} \approx 10^3 \text{ years}, \tag{18c}$$

where 1000 km was used as the length scale, L.

The initial Π contours for both layers as well as the Π_b contours are shown in Figure 8. Planetary islands are evident in both the Π_2 and the Π_b fields. The topography, a Gaussian bump, is centered 180 km SE of the basin's center. This was done to distance the planetary island from the influences of the boundary layers. As mentioned, w_1 and w_2 are equal in strength ($w_1 = w_2 = 5 \times 10^{-7}$ m/s) and uniform in space. From (14a), we see that for this choice of forcing there is essentially no upper layer flow across Π_1 contours in the steady state. Thus, barring any large deformations of the potential vorticity fields, we expect the steady state to show no flow in the upper layer and a flow resembling that of Figure 2c in the lower layer.

b. Boundary layers. Planetary geostrophic dynamics are, of course, not appropriate in the boundary layers and indeed these are highly diffusive in the model. While it was possible to obtain a numerically stable boundary regime by simply enhancing the diffusivity in the zonal direction near the western wall, this proved to seriously limit the allowable time step. Instead, we chose to damp the waves (and forcing) artificially over the 10 westernmost grid points. That is, all terms in (14) of the forms $g_i J(\eta_i,\Pi_i)$ and w_i ($i = 1,2$) were multiplied by factors increasing from zero at the western boundary to unity beyond the tenth grid point. It should be mentioned that this parameterization of

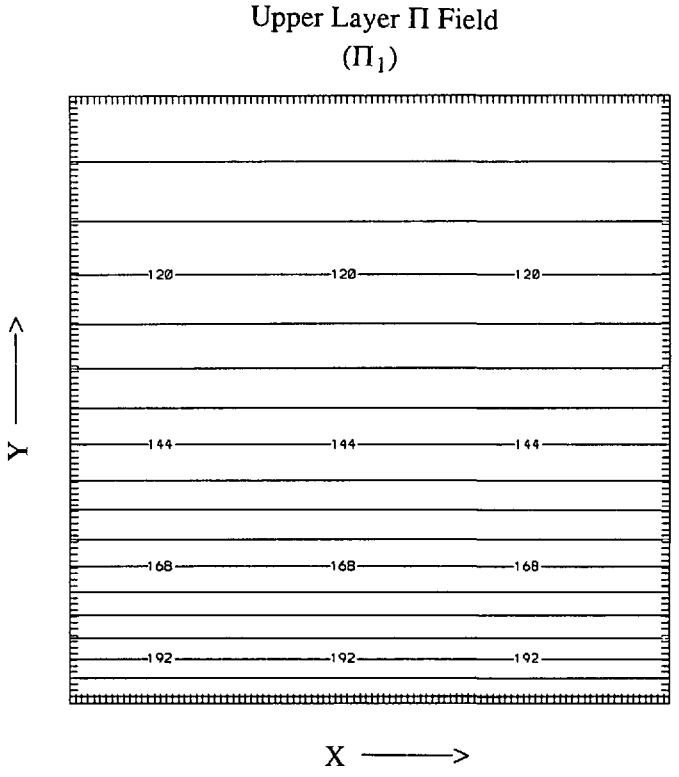

Figure 8. Initial Π ($=d/f$) contours: The inverse potential vorticity is plotted instead of the potential vorticity itself because, in the steady state, Π is proportional to a streamfunction for the characteristic velocity field: (a) for the upper layer and (b) for the lower layer. (c) shows the sum of (a) and (b), the Π_b field.

the western boundary regime acts as a net source of mass for the system. This is because the continuity equation is embedded in the potential vorticity equation which is altered in the western boundary layer. Since both the transient signals and the ultimate steady state characteristics propagate information essentially from east to west and because of the weak level of diffusion used, it is believed that the exact nature of the boundary layer is of only secondary importance to the problem considered here. This is not to suggest, however, that boundary layers would not play a more important role in the subsequent adjustment to a true steady state in a more complete dynamical system.

c. Model results. In the initial stages of the spin up, η_2 is small, $O(\eta_1)$, which since $g_2 << g_1$, implies that the vertically averaged flow, **U**, is well approximated by

$$\mathbf{U} = \frac{g_1}{f}(-\eta_{1y}, \eta_{1x}) \tag{19}$$

Lower Layer Π Field

(Π_2)

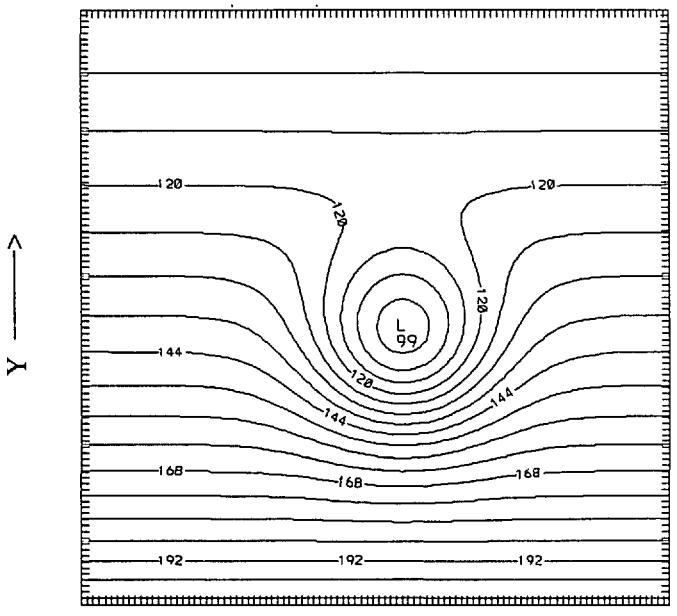

Barotropic Π Field

($\Pi_1 + \Pi_2$)

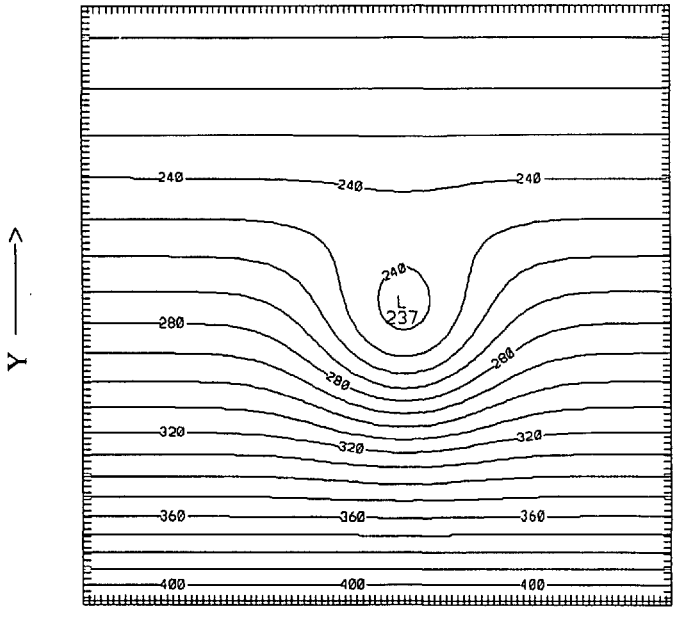

Figure 8. (Continued)

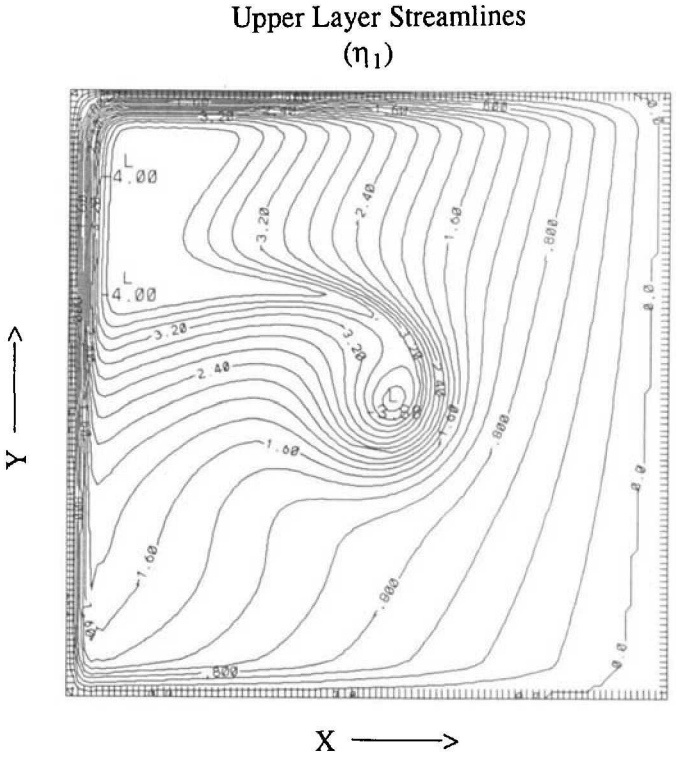

Figure 9. The spin up calculation at $t = 8 \times 10^6$ seconds. (a) upper layer streamlines (b) lower layer streamlines (c) lower interface. The initial ("barotropic") waves have completely crossed the southern part of the basin and have crossed about 4/5 of the basin at its northern boundary. The flow resembles the planetary geostrophic steady state which would be expected for a single layer model forced by w_1 and with depth $d_T = d_1 + d_2$. A weak dipole structure is already apparent in the lower interface height field, however. Figures 9–12 have been smoothed to remove "two-delta x" noise. A similar smoothing was applied periodically throughout the course of the numerical integration.

and that the Jacobian term on the RHS of (15) is small ($O(\epsilon)$). Thus, (15) reduces to

$$\eta_{1t} + g_1' J(\eta_1, \Pi_b) \approx - w_1 + \text{diffusion} \tag{20}$$

and information propagates from the eastern boundary along characteristics described by Π_b. In this manner, the flow field evolves toward a circulation pattern similar to the steady inviscid pattern seen in Figure 2c, except that the relevant Π field is Π_b. This stage of the numerical spin up is shown in Figure 9. At latitudes where there is no topography, this initial barotropic flow (i.e. vertically averaged over the two active layers) will persist until the arrival of the baroclinic wave front from the eastern boundary.

Where there is topography, the initial barotropic response forces a dipole-like

Lower Layer Streamlines

$((g_1/g_2)\eta_1 + \eta_2)$

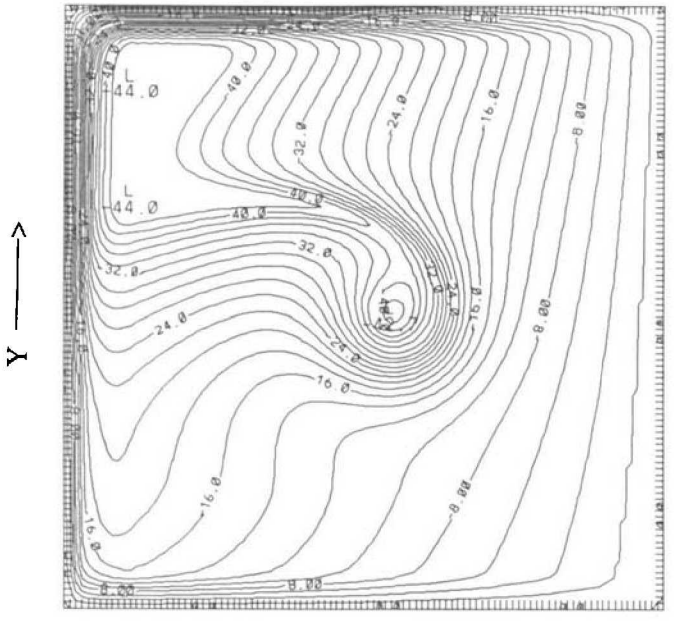

Lower Interface

(η_2)

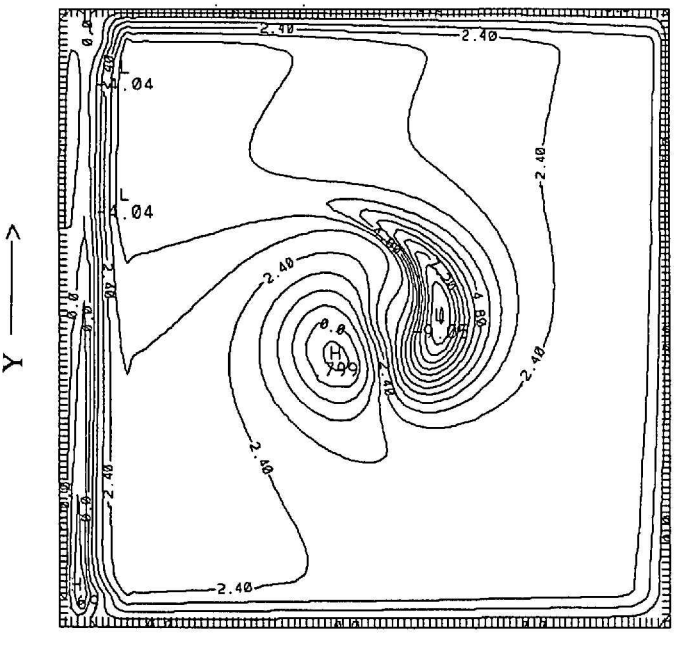

Figure 9. (Continued)

structure in the η_2 field to appear over the topography (Fig. 9c). This large structure is analogous to the initial baroclinic response to the switch on of a subcritical zonal current over topography, such as that recently studied by Rhines (1989). Drawing from Rhines' results, we might expect the "high" to propagate away to the west while the "low" remains permanently bound to the topography. In fact, since a horizontal Laplacian diffusion of the interface height fields is used in the model, the steady state balance inside the closed contour region would seem to require just that. Using an overbar to denote averaging around closed Π_2 contours, the steady state balance for the lower layer yields

$$w_2 = 2R\overline{\nabla^2\eta_2} + 10R\overline{\nabla^2}\eta_1. \tag{21}$$

A positive w_2 thus requires a local minimum of $\eta_2 + 5\eta_1$ inside the closed contours. Owing to the disparity in the density jumps at the two interfaces, η_2 scales like $10\eta_1$ and hence a local minimum in η_2 might also be anticipated. The spin up toward that steady state quickly diverges from the problem studied by Rhines, however, in that there is a strong feedback loop between the baroclinic dipole and the barotropic flow that initially created it.

This feedback stems from a linear, topographic coupling of the fast and slow waves of the system. That is, Eqs. 14a,b (or 14b and 15, etc.) cannot be decoupled, even in their linearized forms.[6] The quick adjustment described by (15) causes a change in the barotropic velocity, **U**. This then leads to changes in the η_2 field as seen by rewriting (14b),

$$\eta_{2t} + \frac{g_2 d_1}{d_T} J(\eta_2, \Pi_2) = -f\mathbf{U} \cdot \nabla\Pi_2 - w_2 + \text{diffusion}. \tag{22}$$

Then, via the Jacobian term on the RHS of (15), η_2 forces η_1 (and hence **U**) on the fast timescale. In this manner, information from the east can penetrate closed contour regions and can reach saddle points. It is interesting that this ability for planetary geostrophic dynamics to communicate information into a closed contour region is lost once the steady state is reached.

The baroclinity introduced by this coupling serves to rid the flow of the strong imprint of the Π_b contours which was evident in Figure 9. Figures 10a-c show the upper and lower layer pressure fields as well as the lower interface height field at time $t = 2.4 \times 10^7$ seconds. The baroclinic wave front has then traversed only a small

6. Nonlinearities in the problem appear in the form of steepening terms (wave speed dependence on signal amplitude) as well as in terms proportional to $J(\eta_1,\eta_2)$. These nonlinearities are generally small, however, in the initial stages of the spin up and a separate experiment showed that the removal of these terms had little effect on the dynamic fields. Also, while it is true that these equations can be separated into linear modes in the WKB sense if a wavelike dependence in the η fields is assumed, the response seen here has length scales of the same order as the topographic scales so that the WKB approximation is not appropriate. Nevertheless, such a decomposition does prove interesting and the resulting dispersion of such waves is presently under investigation.

fraction of the basin and has not yet reached the topography (one can see the front in Figs. 9a and 10a). In spite of this, the flow over the topography is already quite baroclinic. The upper layer flow, for example, readily crosses the region of closed Π_b contours. The northward drift in this region is fed by a relatively intense eastward flow leading from the western boundary layer to the southern edge of the topography. Just west of the topography is a large region of weakened flow. In the lower layer, the flow inside the closed Π_2 contours has been largely shut off, (Fig. 10b). Where the double jet is anticipated in the steady solution, a weak cyclone is seen in the lower layer and a tendency for the flow to deflect eastward and then back westward is seen in the upper layer. That the initial barotropic double jet has been shut off is a consequence of information having reached the saddle point in Π_b.

Figures 11a–c show the flow fields at $t = 2 \times 10^8$ seconds. A small region of relatively intense circulation has developed in the upper layer. This is the result of closed contours forming there as the lower layer drains in the region of closed Π_2 contours. A single (eastward) jet connects the western boundary to this small gyre. Most of the flow in this jet then gradually makes its way northward, essentially conserving its potential vorticity as the lower interface drops beneath it. Above the double jet in the lower layer, there is a westward jet in the upper layer. A remnant of the northeastward drift from the initial barotropic response still occupies the northwestern portion of the basin. The eastward edge of this feature marks the westward penetration of the baroclinic front. In the lower layer, the flow already resembles the anticipated steady state. Comparing Figures 11b and c, it is seen that by this time the pressure field in the lower layer is primarily associated with variations in the lower interface, η_2. An exception to this occurs below the small recirculation in the upper layer. There, the thermal wind shear associated with η_2 serves primarily to shut off the westward part of that recirculation in the lower layer, thus reducing the flow across Q_2 contours inside the planetary island.

Figures 12 and 13 show the pressure, interface height and Π fields at $t = 4.4 \times 10^8$ seconds, the end of the numerical integration. Because of the weak level of diffusion, the system has not yet reached its final steady state inside the planetary island. The baroclinic wave front has, however, traversed the basin. The planetary island in the upper layer is now as large as that in the lower layer. While the closed contours are associated with a maximum of potential vorticity in the lower layer, they are associated with a minimum in the upper layer. The sign of the Q extremum in the upper layer is a consequence of the sign of the forcing and not the sign of the topography. As w_2 continues to drain the lower layer, it depresses the lower interface and creates a local minimum in Q_1. That ∇Q reverses sign with depth suggests a baroclinic instability of the flow in this area and such instabilities would probably be important in a more complete description of the spin up of this region. Outside of the closed contours a double jet system is evident in both layers and the accelerated zonal flow associated with curvature of the Q field is evident in the lower layer. While these features are

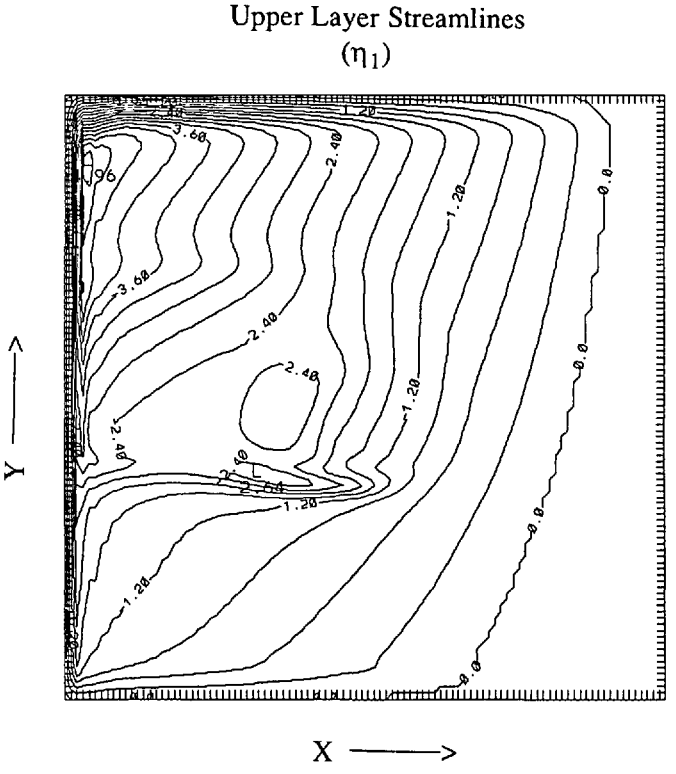

Figure 10. Same as (9) except that $t = 4 \times 10^7$ seconds. By now the flow is quite baroclinic over and just west of the topography. Notice that the baroclinic wave front has not yet reached the topography (recall that upon arrival of the baroclinic wave front, the upper layer flow is shut off). The baroclinization of the flow in the vicinity of the topography is due to a linear, topographic coupling of the potential vorticity equations of the two layers.

strong compared with the traditional SA flow, they are weak compared with the flow inside the closed contours.

4. Summary and discussion

Two models were used to study the effects of isolated topography on the mass driven abyssal circulation. In the first, the inviscid Stommel-Arons problem was solved numerically in two beta-plane basins exhibiting closed contours of rest state potential vorticity. In both cases, the closed contours were isolated (i.e. far from basin boundaries) and thus the outermost closed contour (the separatrix contour) contained a saddle point in potential vorticity. This resulted in a non-removable singularity in the characteristic equation for η, which gave rise to a double jet structure extending between the western boundary and the saddle point and centered on the separatrix contour. The eastward jet reconnected with the westward jet after encircling the closed

Lower Layer Streamlines

$((g_1/g_2)\eta_1 + \eta_2)$

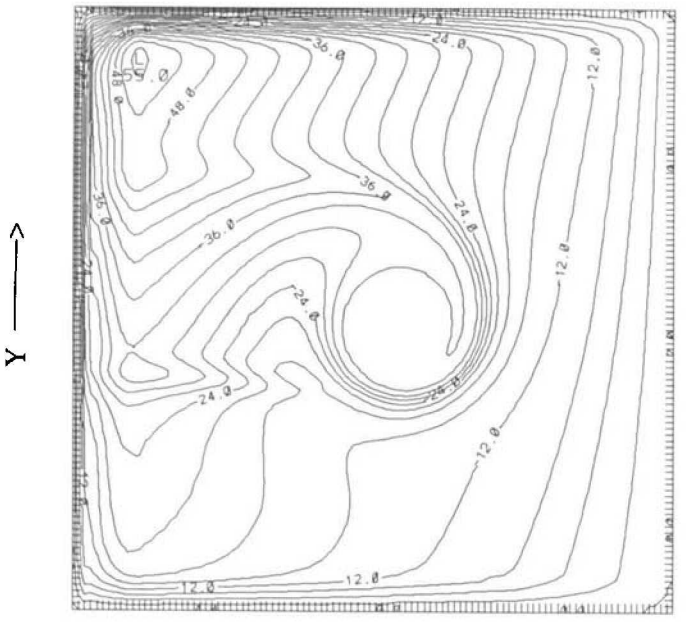

Lower Interface

(η_2)

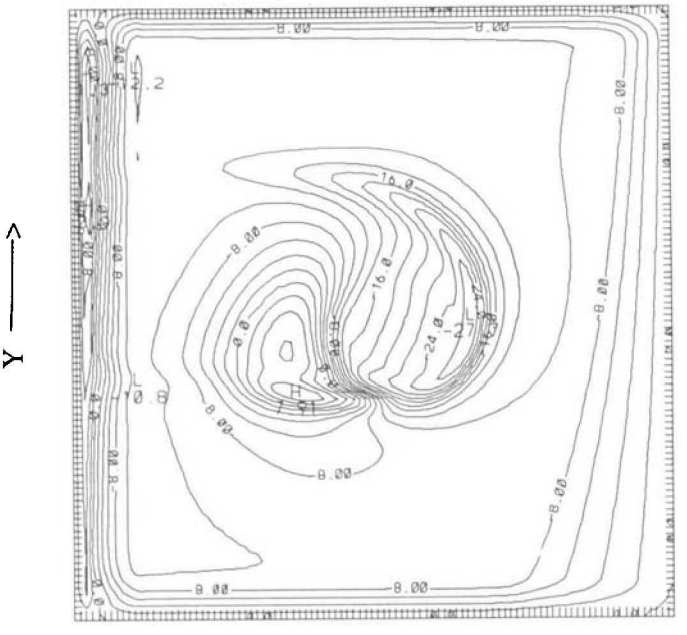

Figure 10. (Continued)

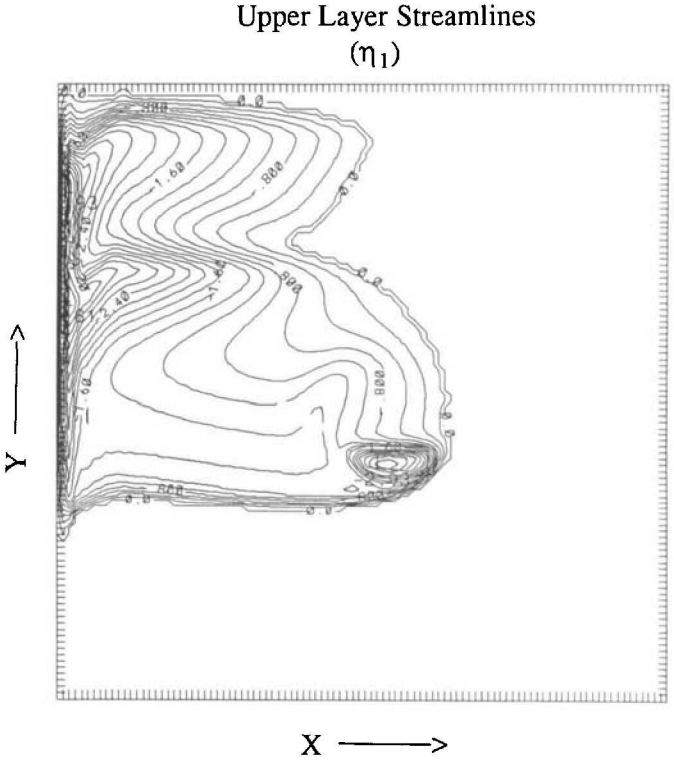

Figure 11. Same as (9) except that $t = 2 \times 10^8$ seconds. By this time the baroclinic wave front has completely traversed the southern portion of the basin. A small recirculation has developed in the upper layer indicating that Q_1 contours have been closed there. Over the closed contours in the lower layer, η_2 continues to drop and will do so until a diffusive balance with the forcing is established. As this interface drops, fluid columns in the upper layer are stretched, resulting in a northward flow. Variations in the η_2 field now account for most of the pressure perturbation seen by the lower layer.

contour region. When connected by an assumed western boundary current, this system of jets represents a recirculation which, in the linear limit of the problem is infinite in strength. The strength of the recirculation is quickly made finite, of course, once diffusive and nonlinear effects are taken into account.

The double jet system described here contrasts the prediction of a single eastward jet by Welander (1969) for a similar problem. This new feature is a consequence of forcing near the saddle point. Thus, if this forcing were identically set to zero, a single jet similar to that predicted by Welander would be expected in its place. Whether a single or double jet system will persist once higher order dynamics is taken into account remains unclear. Since the prediction here is based on equations appropriate to large scale flows, it is hypothesized that result will depend on the breadth of the region of

Lower Layer Streamlines

$((g_1/g_2)\eta_1 + \eta_2)$

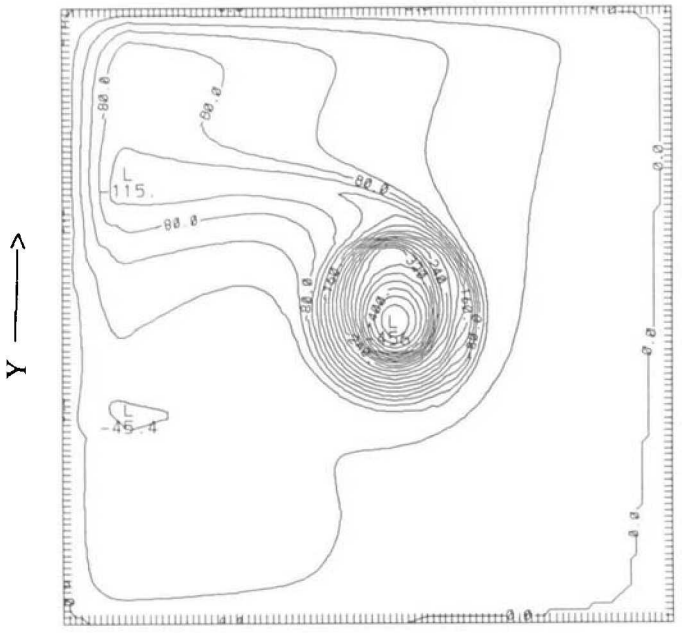

Lower Interface

(η_2)

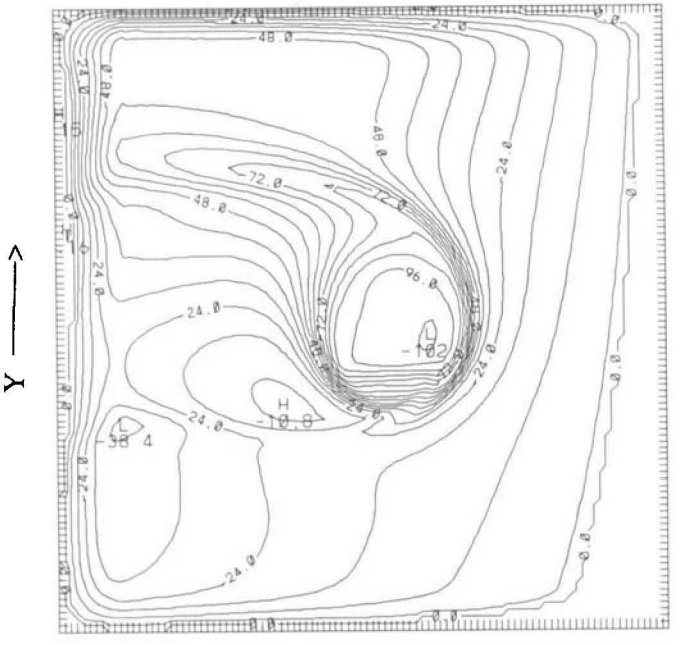

Figure 11. (Continued)

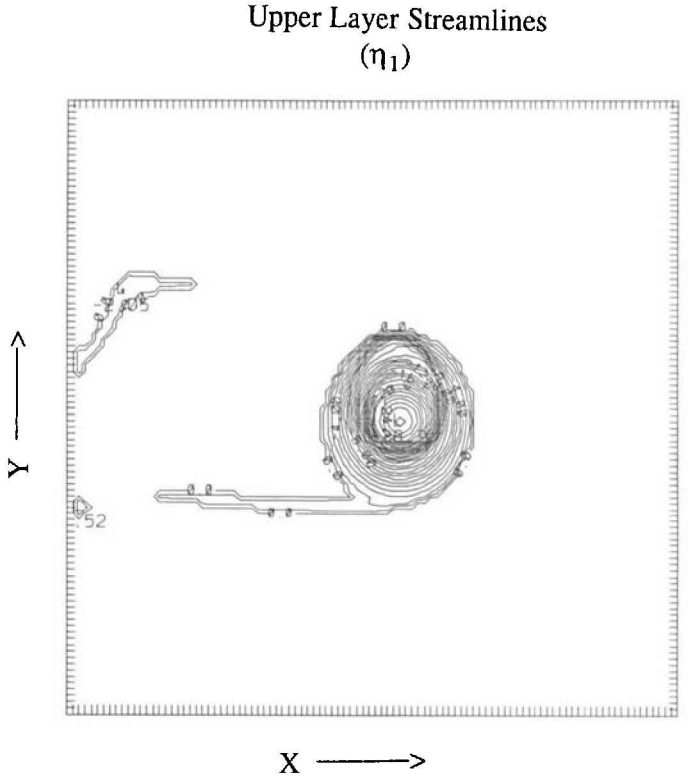

Figure 12. Same as (9) except that $t = 4.4 \times 10^8$ seconds. By this time the baroclinic wave front has completely traversed all of the basin. A double jet system is seen in both layers and a relatively quick zonal flow (similar to that seen in the inviscid calculation (Fig. 2c)) is observed to the west of the closed contours in the lower layer. These flows are, however, weak when compared to the recirculations in the closed contours themselves. The latter flows are, however, very much dependent on the choice of diffusion.

high F near the singularity or, equivalently, on the slowness with which ∇Q approaches zero in the vicinity of the saddle point.

In a related study by Rhines (1989), the effect of horizontal diffusion near saddle points in a $1\frac{1}{2}$ layer, time dependent, planetary geostrophic channel model were considered. His results demonstrated how diffusion near the saddle point could lead to a blocking of a zonal flow. This was accomplished by a ridge in η extending westward from the saddle point. Here, diapycnal forcing near a saddle point was shown to have a similar effect, except that the sign of the forcing was such that a trough, instead of a ridge of η was observed.

The long-geostrophic contour component of the flow results from variations with potential vorticity of either $F\ (=w_i/c)$ or of the distance, following a characteristic, from the eastern boundary. In the flat-bottom case, for example, zonal flow resulted from a $1/f^2$ dependence in the characteristic speed, c. Topography, in addition to

Lower Layer Streamlines

$((g_1/g_2)\eta_1 + \eta_2)$

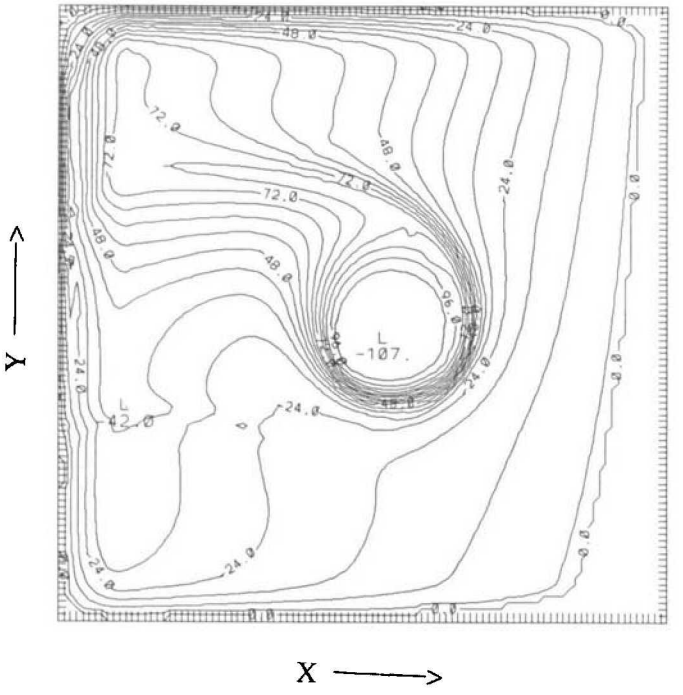

Lower Interface

(η_2)

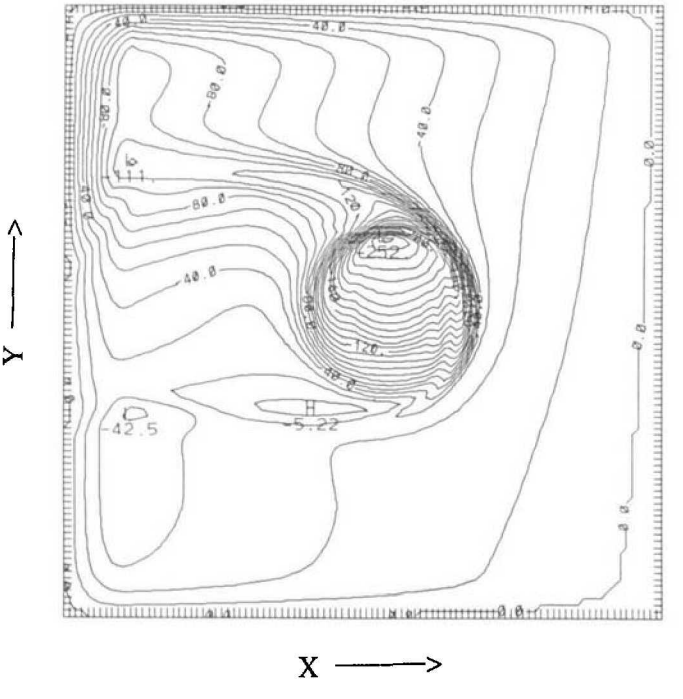

Figure 12. (Continued)

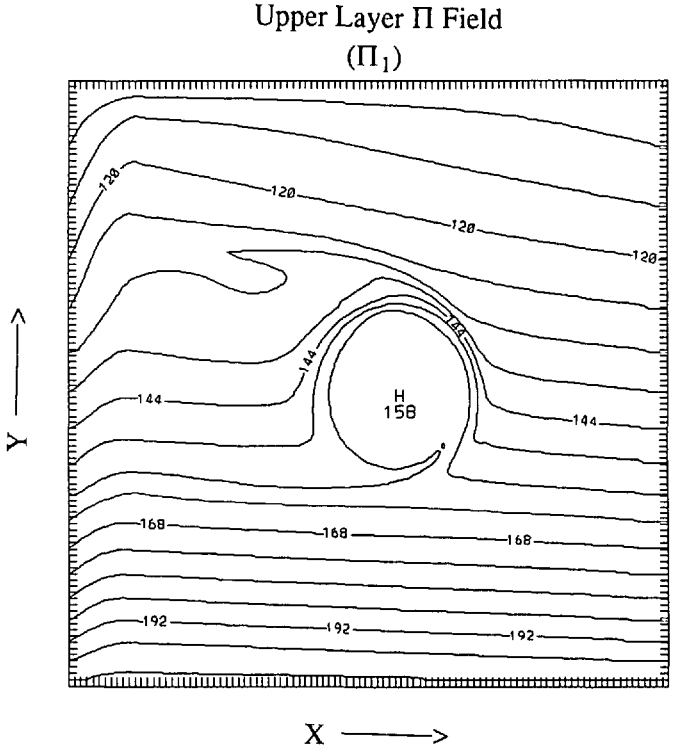

Figure 13. Same as (8a,b), but for $t = 4.4 \times 10^8$ seconds. Qualitatively the Π_2 field remains relatively unchanged, in contrast to the Π_1 field which now also exhibits a planetary island, allowing for a closed circulation in the upper layer.

affecting c, also affects the integration path length. In general, such variations of path length may be related to neighboring characteristics having originated in different parts of the basin's boundary (e.g., the ridge topography problem studied by Cessi and Pedlosky (1986)) or to curvature of the Q field in the basin's interior. Because topography was isolated from sidewalls and w_i was constant in our model, only variations with Q of c and the curvature of the Q field were relevant.

Over most of the latitude band in which topographic effects were important, it was found that excitation of the component of velocity along Q contours (the free flow) originated in a rather limited domain. This result implies that spatial variation about the global mean value of w_i could lead to a reversal or intensification of the free flow. Divergent eddy fluxes of potential vorticity (not considered here) as well as the spatial variability of diapycnal mixing (in a true steady state) could contribute to such spatial variability in the forcing. With respect to the eddy forcing, it would be interesting to study the behavior of smaller scale (e.g., quasi-geostrophic) eddies in the vicinity of curved Q contours in general and near saddle points of Q in particular.

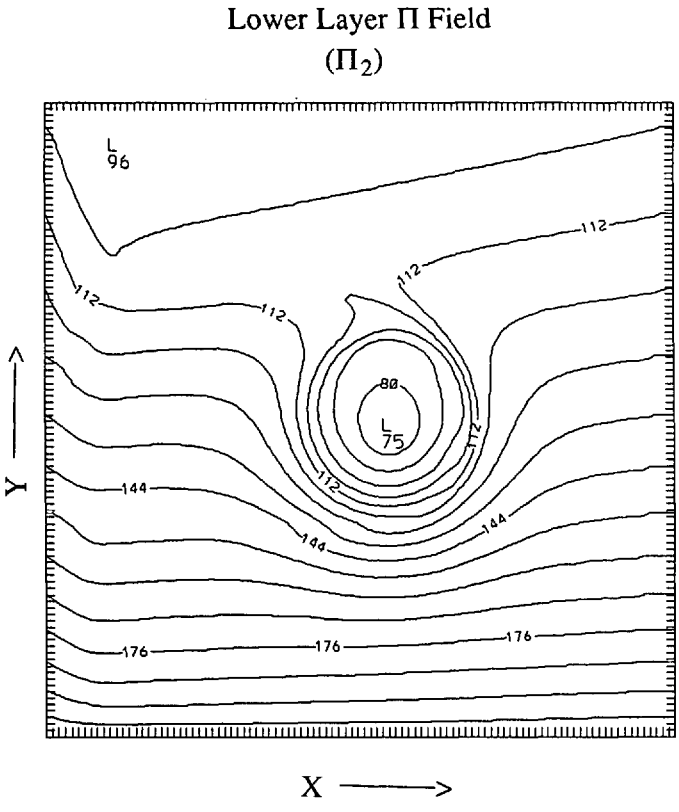

Figure 13. (Continued)

The second model added time dependence and stratification to the first, resulting in a 2½ layer planetary geostrophic model. A relatively large density jump at the upper interface resulted in a separation of time scales. The fast and slow waves were coupled by the topography and it was found that this coupling provided a means for communicating information to closed contour regions as well as to saddle points. This communication serves to feed energy into the baroclinic flow field locally wherever there were zonal variations in topography. In particular, it enabled the flow to readily cross barotropic Q-contours in the upper layer and tended to inhibit flow inside closed Q_2-contours in the lower layer. Similar coupling effects would be expected between the various modes of a multi-layered (or continuously stratified) system. In particular, processes akin to those discussed here might occur in the spin-up of wind driven gyres, particularly in basins possessing planetary islands of barotropic potential vorticity.

The latter stages of the spin up showed closed contours in both layers and these planetary islands of Q, were connected to the western boundary by double jets. The zonal flow was intensified west of the closed contours in the lower layer, as had been predicted by the inviscid theory. The evolving reversal in ∇Q with depth suggests that

the flow inside the closed contours may be baroclinically unstable and a more complete description of the spin up of this region should resolve the eddies ensuing from these instabilities, as these may play a significant role in the horizontal diffusion of Q.

There are numerous regions of the ocean in which rises and basins occur with lateral scales similar to those in these models. Typically, topography has amplitudes much greater than the $O(300$ m) heights discussed here and is not generally isolated from basin sidewalls. This should serve only to increase the role of topography, and there is already evidence of deep flows significantly stronger than SA's predictions in several deep basins (e.g., Reid (1989)) for the Brazil Basin.

Topography may also affect the abyssal circulation in ways more fundamental than those discussed here. A mass source entering a basin (such as that that forced Kawase's model), for example, may be controlled by the hydraulic nature of low through deep passages between basins (e.g. Hogg, 1983). Similarly, topographic slopes near basin sidewalls may alter the Kelvin wave component of the spin-up. The intersection of isopycnals and isobaths pose further complications. The sloping-bottom stratified boundary layer, for example, ceases to have the properties of Ekman layers (Rhines and MacCready, 1989; MacCready and Rhines, 1990), and thus new parameterizations of bottom drag, transverse circulation and interior spin-down must be sought. Finally, Rhines and MacCready (1989) discuss the effect of basin hypsometry (i.e. variation in horizontal area with depth) in conditioning the vertical velocity, and hence the interior general circulation of such basins (there is a strong tendency for anticyclonic interior circulation, opposite in sense to SA predictions).

Acknowledgments. This work benefitted from discussions with Mitsuhiro Kawase, whom we thank. We also thank the San Diego Scientific Computing Center and the National Science Foundation (Grants OCE 84-45194 and 86-13725).

REFERENCES

Cessi, P. and J. Pedlosky. 1986. On the role of topography in the ocean circulation, J. Mar. Res., *44,* 445–471.

Davey, M. K. 1983. A two-level model of a thermally forced ocean basin, J. Phys. Oceanogr., *13,* 169–190.

Hogg, N. 1983. Hydraulic control and flow separation in a multilayered fluid with applications to the Vema Channel. J. Phys. Oceanogr., *13,* 695–708.

Kawase, M. 1987. Establishment of deep ocean circulation driven by deep-water production. J. Phys. Oceanogr., *17,* 2294–2317.

MacCready, P. M. and P. B. Rhines. 1990. Buoyant inhibition of Ekman transport on a slope and its effect on stratified spin-up. J. Fluid Mech. (in press).

Reid, J. L. 1989. On the total geostrophic circulation of the South Atlantic Ocean: Flow patterns, tracers and transports. Prog. in Oceanogr., *23.*

Rhines, P. B. 1989. Deep planetary circulation and topography: Simple models of midocean flows. J. Phys. Oceanogr., *19,* 1449–1470.

Rhines, P. B. and P. M. MacCready. 1989. Boundary control over the general circulation, Proc. 'Aha Hulikoa' Workshop, P. Mueller Ed., Univ. of Hawaii, 75–97.

Stommel, H. and A. B. Arons. 1960a. On the abyssal circulation of the world ocean—I. Stationary planetary flow patterns on a sphere. Deep-Sea Res., *6*, 140–154.

—— 1960b. On the abyssal circulation of the world ocean—II. An idealized model of the circulation pattern and amplitude in oceanic basins. Deep-Sea Res., *6*, 217–233.

Welander, P. 1969. Effects of planetary topography on the deep-sea circulation. Deep-Sea Res., *16*, (suppl.), 369–391.

Received: *24 August, 1989;* revised: *9 February, 1990.*